# Quantum transport with coupled cavities on an Apollonian network

Guilherme M. A. Almeida and Andre M. C. Souza*
*Departamento de Física, Universidade Federal de Sergipe, 49100-000 São Cristóvão, Brazil*
(Received 25 October 2012; published 8 March 2013)

We study the dynamics of single photonic and atomic excitations in the Jaynes-Cummings-Hubbard (JCH) model where the cavities are arranged in an Apollonian network (AN). The existence of a gapped field normal frequency spectrum along with strongly localized eigenstates on the AN highlights many of the features provided by the model. By numerically diagonalizing the JCH Hamiltonian in the single excitation subspace, we evaluate the time evolution of fully localized initial states, for many energy regimes. We provide a detailed description of the photonic quantum walk on the AN and also address how an effective Jaynes-Cummings interaction can be achieved at the strong hopping regime. When the hopping rate and the atom-field coupling strength is of the same order, the excitation is relatively allowed to roam between atomic and photonic degrees of freedom as it propagates. However, different cavities will contribute mostly to one of these components, depending on the detuning and initial conditions, in contrast to the strong atom-field coupling regime, where atomic and photonic modes propagate identically.

DOI: 10.1103/PhysRevA.87.033804 PACS number(s): 42.50.Pq, 42.50.Ex, 03.67.−a, 89.75.Da

## I. INTRODUCTION

Cavity quantum electrodynamics systems have been widely considered as a suitable choice for implementation of quantum information processing schemes [1–4]. The well-known Jaynes-Cummings (JC) model [5] is the most important framework for investigating fundamental aspects of the interaction between light and matter. It describes a two-state atom (qubit) coupled to a single field mode within a highly reflective cavity and it is exactly solvable, within the rotating-wave approximation. Further generalizations of this model include multiple atoms, $N$-level atom, dissipation, and so forth [6].

Experimental advances in optical microcavities [7], photonic crystals [8], and superconducting devices [9] have brought interest to Hubbard-like models where photons can hop through an array of coupled cavity systems [10,11]. An attractive feature provided by such systems is the local addressing of individual cavities, as long as the distance between adjacent cavities is larger than the optical wavelength of the resonant mode. In particular, the Jaynes-Cummings-Hubbard (JCH) model [12] provides a framework for studying quantum many-body phenomena such as phase transitions where strongly correlated photons play the role. Most of recent work has focused on the Mott insulator-superfluid quantum phase transition of polaritons (combined atomic and photonic excitations) [12–21].

As coupled cavity systems allow the control and measurement of individual cavities, these turn out to be a reliable setup for distributed quantum information processing [22] as well, which requires entanglement generation [23] and quantum state transfer between distant nodes in a network [24,25]. Some work has also addressed the propagation dynamics of single excitations in such coupled cavity systems [26–29]. These excitations can be photonic or atomic, where the first travels by direct hopping and the latter by energy exchange with the photonic mode. By considering various energy regimes, Ogden *et al.* [26] studied atomic state transfer between two coupled cavities, each containing a single two-level atom. They found that, by setting the appropriate detuning and hopping parameter, a high-fidelity atomic excitation transfer from one cavity to another can be achieved. Makin *et al.* [27] investigated both atomic and photonic dynamics in a one-dimensional array of coupled cavities. For limiting energy regimes, they showed that the system can be mapped to two uncoupled Heisenberg spin chains. The dynamics turns to be much more complex when the hopping rate and atom-field coupling parameter is of the same order. They have also shown that the pulse dispersion can be attenuated by considering a parabolic distribution of hopping rates, or by encoding the initial state as a Gaussian wave packet. In [29], Dong *et al.* discussed the binary transmission dynamics in a chain of coupled cavities, each containing a tree-level atom, and provided a class of encoding protocol which can improve the state transmission fidelity. In [28], Ciccarello addressed the appearance of an effective JC interaction at the strong hopping regime, for large-size arrays. By considering a staggered pattern of hopping rates, instead of uniform, a gapped discrete field normal frequency in the middle of the band is induced, corresponding to a strongly localized field normal mode. By setting the appropriate parameters, a significant atom-field interaction can persist even if we increase the system size and thus the atomic excitation is no longer frozen.

These results indicate that even in the single excitation subspace, the JCH model presents an appealing dynamics due to the interplay between atomic and photonic degrees of freedom. So far, only regular structures have been considered. Thus it raises the question of whether new features arise if we arrange the cavities in more complex structures.

Lately, a class of networks which are neither completely regular nor completely random, named small-world networks [30], where the average length of the shortest path $l$ between two nodes increases logarithmically with the network size $N$ ($l \propto \ln N$), has been widely studied within many fields, from social and biological systems [30,31] to classical and quantum transport dynamics [32–34]. In particular, a class of complex

*amcsouza@ufs.br

 

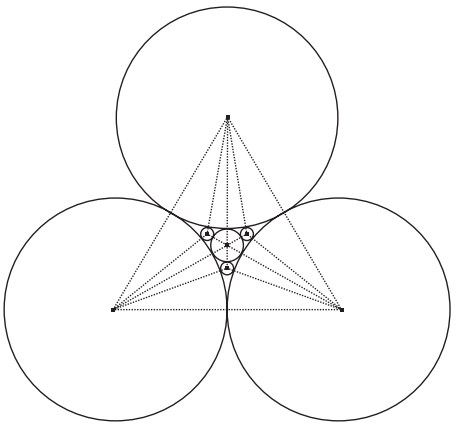

FIG. 1. The second generation ($n = 2$) Apollonian packing (solid lines) and the corresponding AN (dotted lines).

networks called Apollonian networks (ANs) [35], which are simultaneously small world, scale free (that displays a power law degree distribution), and can be embedded in Euclidean space, has brought some attention. The free-electron gas [36], magnetic models [37], tight-biding models [38], correlated electron systems [39], and quantum walks [40] in such networks have been investigated. AN's arise from the problem of space-filling packing of spheres [41]. It can be deterministic or random, and depends on the initial configuration. The most common packing starts with three mutually touching circles. The first generation, $n = 1$, is achieved by inserting a maximal circle in the interstice bounded by the three initial circles. Further generations are obtained by repeating this process for every empty space. This packing can be mapped to the AN as shown in Fig. 1. At a given generation, the number of nodes is given by $N(n) = (3^n + 5)/2$, and the number of connections by $C(n) = (3^{n+1} + 3)/2$ ($n = 0,1,2,\ldots$). In each generation a new group of nodes sharing the same degree $\gamma$ is created. More precisely, there are $3^{n-1},3^{n-2},3^{n-3},\ldots,3^2,3,1$, and 3 nodes with degree $\gamma = 3,3\cdot 2,3\cdot 2^2,\ldots,3\cdot 2^{n-2},3\cdot 2^{n-1}$, and $2^n + 1$, respectively, where the last number represents the three corner nodes. The central node, often referred as the *hub node*, has the largest degree.

In this paper, we study the dynamics of the JCH model where the cavities are arranged in such AN. We numerically diagonalize the Hamiltonian in the single excitation subspace and solve the Schrödinger equation thus obtaining the time evolution of atomic and photonic occupation probabilities in every cavity, for fully localized initial states with one excitation only. We consider three different energy regimes. For the strong hopping case, the photonic component propagates practically free, without significantly exchanging energy with the atomic modes in short time scales. Also, a JC-like interaction can be triggered by setting the appropriate atomic transition frequency and initial conditions. For comparable hopping and atom-field coupling, both JC-like dynamics and/or photonic quantum walk on the AN may be disturbed by the appearance of more complex JCH eigenstates (polaritons). Thus, each cavity might be able to sustain mostly one of both components. When the atom-field coupling strength dominates, atomic and photonic dynamics become identical.

In what follows, Sec. II, we introduce the JCH model. In Sec. III we make an analysis of the free-field Hamiltonian spectrum and eigenstates. In Sec. IV we evaluate the time evolution for a variety of energy regimes and discuss the overall dynamics in terms of the JCH eigenstates. Finally, in Sec. V, we draw our conclusions.

## II. JAYNES-CUMMINGS-HUBBARD MODEL

Let us consider a system of coupled cavities where each occupies the nodes of an Apollonian network. A two-level system $\{|g\rangle,|e\rangle\}$ coupled to a single field mode can be described by the JC Hamiltonian [5,6] (in the rotating wave approximation),

$$h_i^{JC} = \frac{\omega_a}{2}\sigma_z + \omega_f a_i^\dagger a_i + \beta(\sigma_i^+ a_i + \sigma_i^- a_i^\dagger), \tag{1}$$

where $\sigma_z|g\rangle = -|g\rangle$ and $\sigma_z|e\rangle = |e\rangle$, $\sigma_i^+$ ($\sigma_i^-$) and $a_i^\dagger$ ($a_i$) are, respectively, the atomic and photonic raising (lowering) operators for cavity $i$, $\beta$ is the atom-field coupling strength, $\omega_a$ is the atomic transition frequency, $\omega_f$ is the field mode frequency, and we set $\hbar = 1$ for convenience. If we include photon evanescent hopping between nearest-neighbor cavities (tight-binding approximation), we can represent the whole system by the JCH Hamiltonian

$$H = \sum_{i=1}^{N(n)} h_i^{JC} - \kappa \sum_{i,j=1}^{N(n)} A_{ij}^{(n)} a_i^\dagger a_j, \tag{2}$$

where $\kappa$ is the intercavity hopping rate, $N(n)$ is the number of nodes for a given AN generation $n$, and $A_{ij}^{(n)}$ is the adjacency matrix elements. We now restrict the system basis to the single excitation subspace. These excitations can be photonic or atomic, that is $|k\rangle|g,1\rangle$ or $|k\rangle|e,0\rangle$, respectively, where $k \in \{1,\ldots,N(n)\}$ specifies the cavity. As such, the full system state is written as a tensor product of every single cavity state, where one excitation must be conserved (the other nonexcited cavities are in the $|g,0\rangle$ state), so the Hilbert space has $D = 2N(n) = 3^n + 5$ dimensions. In such a basis, the matrix form of Hamiltonian (2) can be simply expressed by [27]

$$H_{1\text{exc}} = \frac{\Delta}{2} I_{N(n)} \otimes Z + \beta I_{N(n)} \otimes X - \kappa A_n \otimes \frac{I_2 + Z}{2}, \tag{3}$$

where $\Delta = \omega_f - \omega_a$ is the detuning between photonic and atomic modes, $I_m$ is the $m \times m$ identity matrix, $X$ and $Z$ are the usual Pauli matrices, and $A_n$ is the adjacency matrix. The ground state $\otimes_{k=1}^{N(n)}|k\rangle|g,0\rangle$ is not included in this subspace, that is, the system is already set with a single excitation.

The AN does not take geometrical deformations into account so we are only interested in the connections between the nodes. By considering uniform intercavity coupling, the adjacency matrix $A_n$ for $n = 2$, for example, can be written by

$$A_2 = \begin{pmatrix} 0 & 1 & 1 & 1 & 1 & 0 & 1 \\ 1 & 0 & 1 & 1 & 0 & 1 & 1 \\ 1 & 1 & 0 & 1 & 0 & 0 & 0 \\ 1 & 1 & 1 & 0 & 1 & 1 & 1 \\ 1 & 0 & 0 & 1 & 0 & 0 & 1 \\ 0 & 1 & 0 & 1 & 0 & 0 & 1 \\ 1 & 1 & 0 & 1 & 1 & 1 & 0 \end{pmatrix} \tag{4}$$

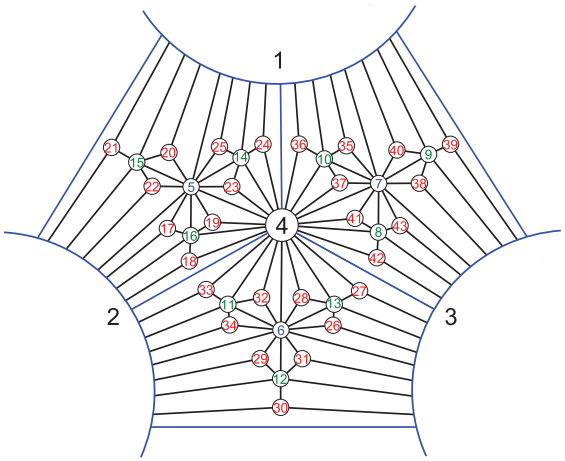


FIG. 2. (Color online) The Apollonian network for $n = 4$ (43 nodes). The first generation is made up by nodes 1–4, the second one includes 5–7, the third, 8–16, and the fourth, 17–43. The corner nodes were drawn bigger for a clearer visualization. This is the node labeling we will adopt through the paper.

(see Fig. 1). In order to discuss our results in the following sections, we need the appropriate identification of each node (cavity), then Fig. 2 provides the node numbering we are going to consider herein, up to the fourth generation AN.

### III. SPECTRUM AND LOCALIZATION PROPERTIES

The JCH model eigenstates are known as polaritons, superposition of atomic and photonic excitations over the entire lattice. As we are considering the single excitation subspace, the polaritons are linear combinations written on the $\{|k\rangle|g,1\rangle, |k\rangle|e,0\rangle\}$ basis, as seen in the last section.

The AN topology induces both localized and extended eigenstates, and its spectrum is characterized by several regions, some of these with a high degree of degeneracy due to the node degree distribution (see Fig. 2). Such configuration drastically changes the way atomic and photonic degrees of freedom relate with each other for specific sets of parameters, comparing to the JCH model defined in regular lattices. Hence, in order to get an idea of the form such polaritons will take, we shall provide a brief description of the free-field Hamiltonian,

$$H_{\text{field}} = \omega_f \sum_{i=1}^{N(n)} a_i^\dagger a_i - \kappa \sum_{i,j=1}^{N(n)} A_{ij}^{(n)} a_i^\dagger a_j, \tag{5}$$

normal frequency spectrum, and eigenstates on the single-photon basis. We solve the above Hamiltonian by numerical diagonalization. In order to characterize the degree of localization of such eigenstates we evaluate the participation ratio, defined as

$$\xi_j = \frac{1}{\sum_{i=1}^{N(n)} |\langle i|\phi_j\rangle|^4}, \tag{6}$$

for a given AN generation $n$, where $|\phi_j\rangle$ represents an eigenstate and $|i\rangle$ is a single photon located at node $i$. This quantity can assume values within 1 for completely localized states and $N$ for extended states ($\langle i|\phi_j\rangle = 1/\sqrt{N}$ for all $i$).

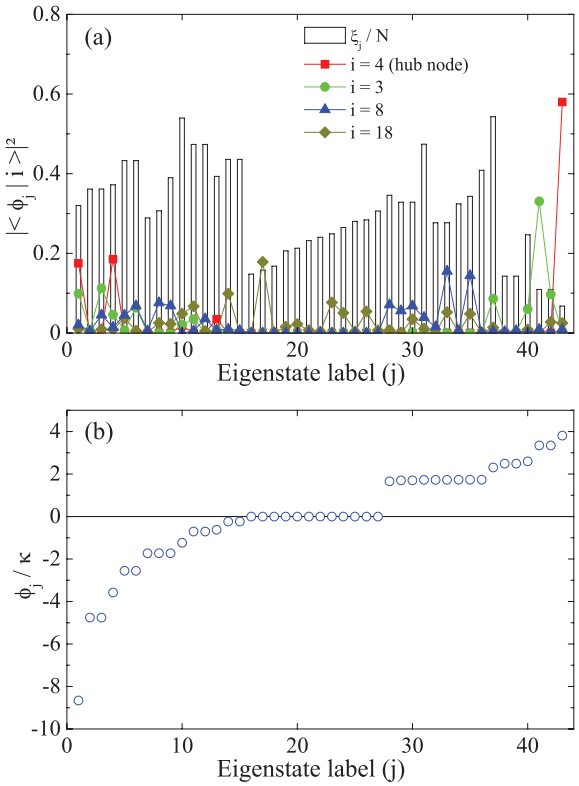


FIG. 3. (Color online) (a) The normalized participation ratio of eigenstates $\xi_j/N$ (column bars) of $H_{\text{field}}$ and the node coefficient amplitudes, $|\langle\phi_j|i\rangle|^2$, for $i = 4$, 3, 8, and 18 on the $n = 4$ AN (43 nodes). (b) The field normal-mode frequency band ($\omega_f = 0$). The eigenstates are labeled according to increasing values of $\phi_j$ (in units of $\kappa$) and, within each degenerate group, by increasing values of $\xi_j/N$.

In Fig. 3(a) we compare the participation ratio with the node coefficient amplitudes, $|\langle\phi_j|i\rangle|^2$, for different $i$'s on the fourth generation AN. It gives us an outlook on the way these states are distributed along the spectrum. The associated field normal-mode frequencies $\phi_j$ are shown in Fig. 3(b), for $\omega_f = 0$ (in units of $\kappa$). First, notice that the hub node $i = 4$, with degree $\gamma = 24$, has its largest amplitude in the most localized eigenstate, $\xi_{j=43}/N \approx 0.07$, corresponding to the frequency $\phi_{j=43}/\kappa \approx 3.8$, which is nondegenerate. From now on, we call it $\phi^{\text{hub}}$. For the other nodes, $i = 3$, 8, and 18, representing the $\gamma = 17$, 6, and 3 group, respectively, more eigenstates get involved but there is still a peak over a reasonable localized eigenstate. It turns out that a similar distribution occurs for every node $i$, with different localization strengths, not necessarily scaling with $\gamma$, although the hub node localized eigenstate will always be paramount, regardless of the network size. Moreover, even within a node group sharing the same $\gamma$, there can be a difference in such localization strengths, since there can be many symmetry groups in it (the AN has a $2\pi/3$ rotational symmetry). Anyway, what is most relevant to be addressed here is that, apart from the hub node localized eigenstate that corresponds to a nondegenerate frequency $\phi^{\text{hub}}$, every node has a (not solely) related localized eigenstate associated with a degenerate frequency level ($\phi_j/\kappa \gtrsim 0$) depending on $\gamma$ (higher frequencies are associated with higher

$\gamma$ values). By looking at Figs. 3(a) and 3(b) we can identify the level $\phi_j/\kappa = 0$ as being related to the $\gamma = 3$ group (nodes 17–43), for instance. Frequencies below this value comprise extended eigenstates mostly.

Although we have only discussed the $n = 4$ AN spectrum properties, the AN structure presents self-similarity as the generation increases and thus it reflects on its properties. These spectrum regions containing strongly localized eigenstates for a given $\gamma$ yield to attractive features when we consider the full JCH Hamiltonian as we are going to show in the next section. Further details about localized and extended states on the AN and its relationship with the structure size and characteristic spectrum, for a similar tight-binding Hamiltonian, can be found in Ref. [38].

## IV. TIME EVOLUTION

In this section we display the results for time evolution of the JCH model arranged on the considered AN. The system eigenstates $|E_j\rangle$ (polaritons) and its corresponding eigenvalues $E_j$ were evaluated by means of numerical diagonalization of Hamiltonian (3). For an initial state of the form $|\psi_k(0)\rangle = |k\rangle \otimes (\cos\alpha|g,1\rangle + \sin\alpha|e,0\rangle)$ fully localized at node (cavity) $k$, we discuss the system dynamics for different energy regimes. The state at time $t$ is given by $|\psi(t)\rangle = U(t)|\psi(0)\rangle$, where $U(t) = e^{-iHt}$ is the quantum time evolution operator. We are primarily interested on the single excitation propagation dynamics. Then for a given initial state $|\psi_k(0)\rangle$, we write

$$\pi_{\ell k}^{ph}(t) = \left| \sum_j^D e^{-iE_j t} \langle \psi_k(0)|E_j\rangle \langle E_j|\ell,g\rangle \right|^2, \tag{7}$$

$$\pi_{\ell k}^{at}(t) = \left| \sum_j^D e^{-iE_j t} \langle \psi_k(0)|E_j\rangle \langle E_j|\ell,e\rangle \right|^2, \tag{8}$$

as the probability of finding the photonic and atomic excitations, respectively, at node $\ell$ in time $t$, where we have denoted $|\ell,g\rangle \equiv |\ell\rangle|g,1\rangle$ and $|\ell,e\rangle \equiv |\ell\rangle|e,0\rangle$.

### A. Strong hopping regime

First, we investigate the strong hopping regime, $\kappa \gg \beta$. In this case, the existence of discrete field normal-mode frequencies along with strongly localized eigenstates brings an interesting feature: a JC-like interaction between the field normal mode and its atomic analog occur for an appropriate tuning of the atomic transition frequency $\omega_a$, regardless of the system size [28], since the AN maintain its spectrum pattern as the generation increases. It means that the atomic component still can propagate (in a time scale of the order of $\beta$) even in such a regime where the atom-field interaction rate is much slower than the photon intercavity hopping. This property comes from the fact that, as long as the single cavity parameters are uniform through the lattice and the decoupling of the hopping Hamiltonian in terms of normal modes is known, the JCH Hamiltonian can be rearranged into a sum of decoupled JC models, each coupling a field normal mode to its atomic counterpart [26–28]. In other words, when $\kappa \gg \beta$, we have well defined atomiclike and photoniclike polaritons, i.e., eigenstates where $\langle i,g|E_j\rangle$ and $\langle i,e|E_j\rangle$ is null, respectively,

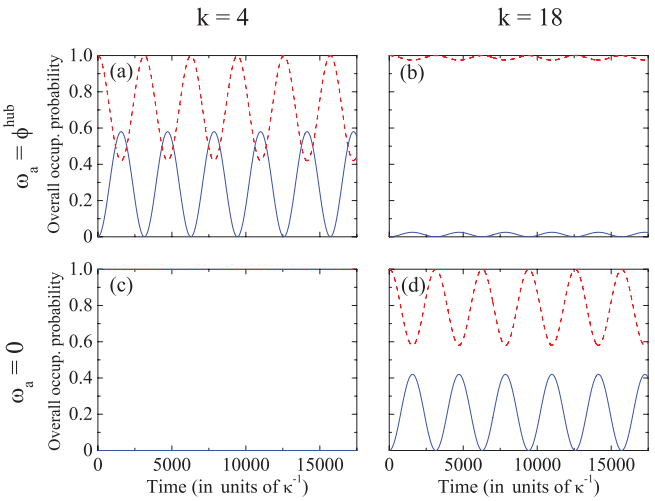


FIG. 4. (Color online) Photonic (solid line) and atomic (dashed line) overall occupation probabilities $\sum_\ell \pi_{\ell k}^{\text{type}}$ for a fully atomic initial state $|\psi_k(0)\rangle = |k,e\rangle$ on the $n = 4$ AN. System parameters are $\kappa/\beta = 10^3$ and $\omega_f = 0$.

for every node $i$. By a judicious tuning of the atomic frequency to a discrete nondenegerate field normal-mode frequency, a pair of such polaritons starts to overlap with both components, by a similar way as the single cavity JC model eigenstates [5,6] except that, in the JCH model, it extends over the entire network. If the field normal-mode frequency happens to be $n$-fold degenerate, then $n$ pairs of polaritons get involved in such a process. Although in this case there is no JC-like interaction exclusively between one field normal mode and its atomic analog, a significant energy transfer between atomic and photonic degrees of freedom might still occur as long as a pair of localized JC-like polaritons is available and we set the appropriate initial state. In order to highlight these phenomena, mainly to address the amount of energy that can be exchanged between atomic and photonic components, for given initial conditions, we shall start the system with a fully localized atomic state. As such, we induce the system dynamics to be generated only by those JC-like polaritons, for the given atomic frequency, and thus the photonic component does not propagate freely. In Figs. 4(a) and 4(b) we show the overall photonic (atomic) occupation probability, $\sum_\ell \pi_{\ell k}^{ph}$ ($\sum_\ell \pi_{\ell k}^{at}$), when the system starts with an atomic excitation at nodes 4 (hub node) and 18, respectively. The atomic frequency $\omega_a$ was set to $\phi^{\text{hub}}$ in order to simulate the dynamics of the JC-like polaritons strongly localized at the hub node. Observe that a significant atom-field interaction happens only when the atomic excitation is initially present at such node. In Fig. 5 we show how the process takes place in a detailed way. The initial concentrated atomic energy is progressively converted into field modes (mostly at node 4) and it reaches the other cavities as well. Right after the field modes reach its maximum, it releases energy until the point that the system is fully atomic again, but the excitation is delocalized instead of being fully localized at the initial node. Then a reverse process occur, i.e., the field modes retrieve the same amount of energy and transfer all of it to the node 4 in the form of atomic excitation, thus recovering the initial state. As long as $\kappa/\beta$ is high enough

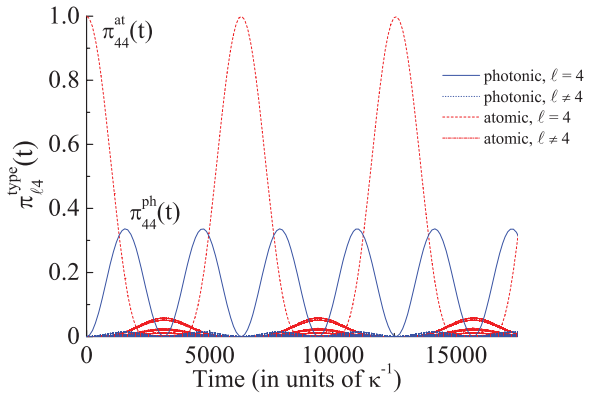


FIG. 5. (Color online) Photonic and atomic occupation probabilities for a fully atomic initial state $|\psi_4(0)\rangle = |4,e\rangle$ on the $n = 4$ AN. Most relevant probabilities are indicated on the figure. System parameters are $\kappa/\beta = 10^3$, $\omega_a = \phi^{\text{hub}}$, and $\omega_f = 0$.

and $\omega_a$ is precisely adjusted to the discrete field normal-mode frequency, the same behavior occurs cyclically. In Figs. 4(c) and 4(d), the atomic frequency matches with the degenerate field normal-mode frequency level comprising every localized polariton associated to the $\gamma = 3$ node group. In this case, as we prepare the atomic excitation at node 4, it freezes [Fig. 4(c)], indicating that the overlap between this node and every involved JC-like polariton is minimum. The same does not apply to node 18 and thus a considerable atom-photon interaction is triggered [Fig. 4(d)]. Even though now there are many polaritons taking part on the dynamics (as the discrete field normal-mode frequency level is degenerated), the atom-field interaction occurs in a similar way as in Fig. 5, since most of the contribution comes from the localized polaritons. Thus, despite the degeneracy degree of a discrete field normal-mode frequency level, we can assert that the overlap between the involved JC-like polaritons and the initial state dictates the amount of energy which can be exchanged. This property is still valid for large-size networks since the AN field normal frequency band is characteristically gapped for any generation. Observe that, in principle, such effective JC interaction is possible in small regular clusters with uniform hopping rates, for instance. However, as we increase its size, the field normal spectrum tends to a continuum thus making an accurate resonance not achievable anymore. In addition, the involved polaritons become even more extended. Therefore, it does not matter in which node we set the initial state, the atomic component becomes practically frozen [27].

Let us now consider an initial state of the form

$$|\psi_k(0)\rangle = |k\rangle \otimes (|g,1\rangle + |e,0\rangle)/\sqrt{2}, \tag{9}$$

which is a JC model single cavity eigenstate [5,6]. In this case, the whole frequency band is available for the photonic mode propagation while the atomic mode behavior depends on the atomic frequency $\omega_a$, in a similar way as in the previous discussion where the initial state was fully atomic. Thus, the photonic mode describes a quantum walk through the network [40] while the atom-field interaction takes place in a much longer time scale, since $\kappa \gg \beta$. Obviously, the latter is only possible if the atomic frequency matches with any of the field normal-mode frequencies. Anyway, regardless of $\omega_a$,

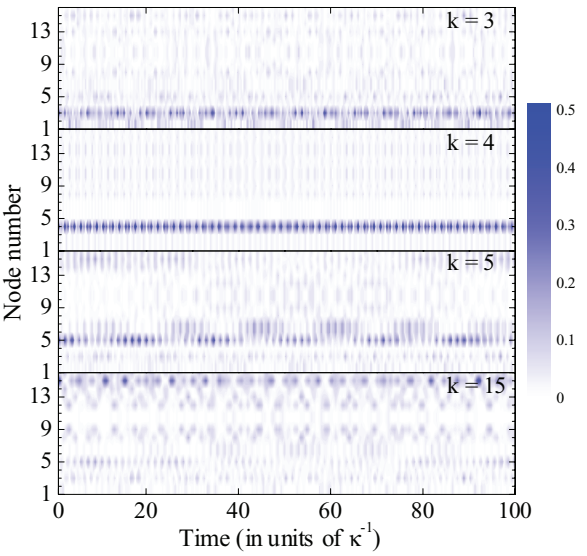


FIG. 6. (Color online) Time evolution of the photonic excitation occupation probability, $\pi^{ph}_{\ell k}(t)$, through the $n = 3$ AN (16 nodes) for the strong hopping regime. The vertical axis represents the occupation probability of a particular node (cavity). The single cavity initial state $|\psi_k(0)\rangle = |k\rangle \otimes (|g,1\rangle + |e,0\rangle)/\sqrt{2}$ is prepared at nodes $k = 3$, 4, 5, and 15. System parameters are $\kappa/\beta = 10^3$, $\omega_a = 0$, and $\omega_f = 0$. The node numbering is available in Fig. 2.

in this case the photonic mode propagates practically freely without being disturbed by the atom-field interaction. Hence, in the remaining of this section we discuss the quantum transport properties of the photonic excitation on the AN.

First, observe that the AN has a $2\pi/3$ rotational symmetry, thus there are several subsets of equivalent nodes (see Fig. 2) like $\{1,2,3\}$, $\{5,6,7\}$, $\{8,10,11,13,14,16\}$, and so forth, in which $|\psi_k(0)\rangle$ would lead to the same dynamics. Likewise, for the initial state set at the hub node ($k = 4$), the occupation probabilities $\pi^{\text{type}}_{\ell 4}(t)$ are equal for each subset. Figures 6 and 7 show the time evolution of the photonic occupation

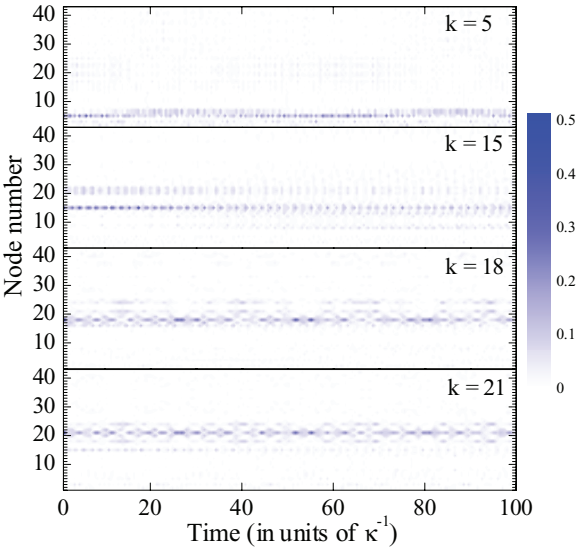


FIG. 7. (Color online) Same as Fig. 6, but for $n = 4$ (43 nodes) and $k = 5$, 15, 18, and 21.

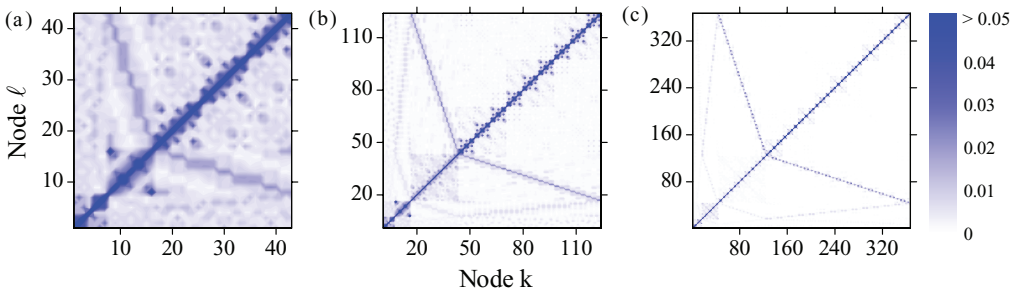


FIG. 8. (Color online) Photonic long-time average occupation probabilities $\chi^{ph}_{\ell k}$ for (a) $n = 4$ (43 nodes), (b) $n = 5$ (124 nodes), and (c) $n = 6$ (367 nodes). System parameters are $\kappa/\beta = 10^3$, $\omega_a = 0$, and $\omega_f = 0$. The plot shape is symmetrical since $\chi^{ph}_{\ell k} = \chi^{ph}_{k\ell}$ for every $k$ and $\ell$, and the highest values are $\chi^{ph}_{kk}$, i.e., the average return probability. Although we have not provided the node numbering for nodes from generations higher than $n = 4$, the purpose here is to give an idea of how the subnetworks and nodes from different generations are connected among themselves. In each generation above, the darkest branch represents the average excitation transport probability between nodes from the current generation and the previous one. The square boundaries point out connections between nodes having the same $\gamma$.

probability for different initial single cavity states on the $n = 3$ and $n = 4$ AN, respectively. Although exhibiting a rather complex dynamics, we can identify some general aspects of the propagation. The most remarkable feature is periodic transition between localized and extended states. The return probability $\pi^{ph}_{kk}$ can reach the highest values so that the excitation is most likely to be found in the initial node. This is expected due to the existence of many localized eigenstates, as discussed in Sec. III. This localization is stronger for $k = 4$, the hub node.

Now let us turn our attention to the probability of finding the excitation in nodes other than the initial one. In general, such probabilities are very small compared to $\pi^{ph}_{kk}$, although these can reach relevant values in some specific nodes. The probability distribution strongly depends on the given AN generation and the initial conditions. In Fig. 6, by examining $\pi^{ph}_{\ell k}$ for $k = 3$, we see that a significant amount of probability flows to the other nodes belonging to the same degree group, that is, nodes 1 and 2. The same applies to $\pi^{ph}_{65}$ and $\pi^{ph}_{75}$ when $k = 5$. For $k = 15$, the nodes 10 and 11, even belonging to the same degree group, are barely populated. It suggests that sharing the same degree does not necessarily imply in privileged networking. It turns clearer in Fig. 7, when $k = 18$ and 21, where the excitation mostly spreads to a few nodes within the subnetwork [42] generated by the new corner nodes 1, 2, and 4. When $k = 5$ for $n = 4$, the excitation still roams between nodes 6 and 7, but now avoiding transport to higher generation nodes. For $k = 15$, there is a relevant probability of finding the excitation at nodes 20, 21, and 22. These nodes belong to the subnetwork formed by nodes 1, 2, and 5, where node 15 plays the role of hub node. These observations indicate that these subnetworks have a fundamental part on the system transport dynamics for higher AN generations.

A better way to visualize how the excitation probability is distributed among the nodes for given initial conditions is by evaluating the long-time average of $\pi^{ph}_{\ell k}(t)$, defined as

$$\begin{aligned}\chi^{ph}_{\ell k} &= \lim_{T\to\infty}\frac{1}{T}\int_0^T \pi^{ph}_{\ell k}(t)dt \\ &= \sum_{i,j}\delta(E_i - E_j)\langle \ell, g|E_i\rangle\langle E_i|\psi_k(0)\rangle \\ &\quad\times\langle\psi_k(0)|E_j\rangle\langle E_j|\ell, g\rangle, \end{aligned} \tag{10}$$

where $\delta(E_i - E_j) = 1$ for $E_i = E_j$ and $\delta(E_i - E_j) = 0$ else. Figure 8 shows the distribution of this average for different AN generations. First of all, notice that $\chi^{ph}_{\ell k} = \chi^{ph}_{k\ell}$ for every $k$ and $\ell$ (since the evolution is unitary), hence this quantity provides us a clearer view on the way the nodes establish communication channels with each other. As it must be, the higher averages are $\chi^{ph}_{kk}$, however, by looking at the other connections we can identify several zones (square boundaries) and branches apart which, interestingly, present self-similarity as $n$ increases. The branches connect generations with each other while the zones connect nodes from the same generation, i.e., with same degree $\gamma$. The strongest (darkest) branch is always the one connecting nodes from the current generation to the previous one. It mostly represents the links between the corresponding hub nodes from the $3^{n-2}$ subnetworks having seven nodes, to its three nearest-neighbor nodes with $\gamma = 3$. As $n$ increases, the previous branches still remain but with lower intensities since the aforementioned hub nodes now have a higher $\gamma$. Also, nodes from "distant" generations seem to be barely connected and links between nodes from the same generation are only relevant within subnetworks composed by 16 nodes at most. For instance, at a given generation $n$, there are $3^{n-m}$ subnetworks having $(3^m + 5)/2$ nodes. Further, these degree interconnections also become weaker as generation increases.

### B. JCH and strong atom-field coupling regimes

In what follows we consider the situation where the hopping rate and the atom-field coupling strength are of the same order: the JCH regime ($\kappa \approx \beta$). In this case the dynamics is nontrivial since there is neither a JC-like interaction between photonic and atomic components nor does the photonic mode describe a quantum walk on the AN, as we have just seen for the strong hopping regime. Instead, somehow both degrees of freedom start to interfere with each other.

At the strong hopping regime it is possible to drive the atomic frequency (comprising a set of denegerate eigenvalues) along the JCH spectrum thus creating JC-like polaritons. Otherwise we have well defined photoniclike and atomiclike polaritons. Once the atom-field coupling parameter is raised, such effective resonance is no longer feasible. In other words,

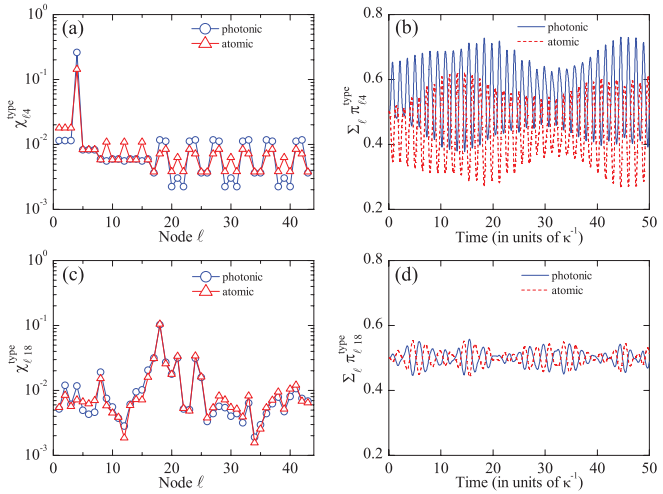


FIG. 9. (Color online) Panels (a) and (c) show the photonic and atomic long-time average occupation probability distribution for $|\psi_k(0)\rangle = |k\rangle \otimes (|g,1\rangle + |e,0\rangle)/\sqrt{2}$ prepared at $k = 4$ and $k = 18$, respectively, and (b) and (d) show the corresponding overall photonic and atomic overall probabilities. System parameters are $n = 4$, $\kappa/\beta = 1$, $\omega_a = 0$, and $\omega_f = 0$. The return average probabilities are $\chi_{44}^{ph} \approx 0.26$, $\chi_{44}^{at} \approx 0.14$, $\chi_{1818}^{ph} \approx 0.103$, and $\chi_{1818}^{at} \approx 0.105$.

at the JCH regime it is not possible to generate a JC-like interaction without disturbing other polaritons associated with different frequency levels on the JCH spectrum, within a range compatible with the $\kappa/\beta$ value. Thus, the excitation roams between photonic and atomic degrees of freedom while it propagates through the network in a rather complex way. It turns out that each cavity provides its contribution mostly to one of these two components, depending on the detuning and the system initial conditions. Hence, an initial state like $|\psi_k(0)\rangle = |k\rangle \otimes (|g,1\rangle + |e,0\rangle)/\sqrt{2}$ will not maintain the even superposition between the whole photonic and atomic parts of the system, as in the strong hopping case. Due to the existence of strongly localized polaritons, we must expect that the detuning and the initial state will be crucial in driving the whole system among both degrees of freedom.

Figure 9 describes how the initial state significantly changes the way each cavity contributes to each one of the components, at the JCH regime. In Fig. 9(a) we show the long-time average occupation probability distribution $\chi_{\ell k}^{\text{type}}$ when the single cavity state is set at the hub node, $k = 4$. Notice that $\chi_{k\ell}^{at}$ can be evaluated by the same way as Eq. (10) by projecting the eigenstates on $|\ell,e\rangle$, instead of $|\ell,g\rangle$. We can see that some groups of nodes have higher $\chi_{\ell 4}^{ph}$ values (including the hub node), others mostly contribute to $\chi_{\ell 4}^{at}$, and a few practically remain even for both components. In Fig. 9(b) we plot the overall photonic (atomic) occupation probability, $\sum_\ell \pi_{\ell k}^{ph}$ ($\sum_\ell \pi_{\ell k}^{at}$). The whole system notoriously fluctuates between both components, mainly due to large shift between $\chi_{44}^{ph}$ and $\chi_{44}^{at}$ plus the fact that the polaritons leading the dynamics are strongly localized. Figures 9(c) and 9(d) show the same quantities but now for $k = 18$ ($\gamma = 3$). Recall that, as $\omega_a = 0$, several pairs of localized JC-like polaritons related to every node with $\gamma = 3$ are involved thus keeping $\chi_{1818}^{ph}$ and $\chi_{1818}^{at}$ practically the same. However, even with a JC-like dynamics taking place, thus resulting in a small variation of the overall occupation probability, other polaritons are involved, hence shifting the average for the rest of the cavities.

Such nontrivial features arising from the JCH regime fade out if we keep on raising the atom-field coupling strength until $\kappa \ll \beta$. In this regime, the dynamics for both atomic and photonic modes behaves exactly like at the large hopping regime but now creating new single cavity eigenstates [if $|\psi_k(0)\rangle = |k\rangle \otimes (|g,1\rangle + |e,0\rangle)/\sqrt{2}$], as passing by other cavities, and propagating at half the speed of the photonic excitation at the $\kappa \gg \beta$ regime [27]. It turns out to be expected, from the fact that, as $\kappa/\beta$ decreases, more JC-like pairs of polaritons are created until the entire JCH spectrum is affected.

### C. Results overview

We now provide a review of the main features provided by the different energy regimes, as previously discussed. Although we have dealt with the JCH dynamics on the AN, these properties apply for any structure. The main difference lies on the existence of a gapped spectrum and localized eigenstates, and also whether or not it holds for a large-size system.

In Fig. 10 we outline the energy regime transition from $\kappa/\beta = 10^3$ to $10^{-3}$ by evaluating the time evolution of the photonic [Fig. 10(a)] and atomic [Fig. 10(b)] return probabilities $\pi_{44}^{\text{type}}$ for a single cavity initial state, Eq. (9). At the strong hopping regime, $\kappa \gg \beta$, the interaction between photonic and atomic components occurs in a time scale much longer than the photon hopping. It means that, in a single cavity initial state, the whole system remains in an even superposition between both components. As the single photon describes a quantum walk through the network, the atom-field coupling does not interfere on it, practically. Moreover, the atomic dynamics will be restricted to a single or a set of JC-like pairs of polaritons (if the corresponding energy level is degenerate), or none, if the atomic frequency $\omega_a$ does not match with any field normal-mode frequency. The latter case is obviously implied in the atomic freezing. On the contrary, a JC-like pair (or pairs) of polaritons might be created and, if it happens that it is strongly localized at some node, by setting the appropriate initial state, a significant atom-field energy exchange takes place (in a time scale of the order of $\beta$), as described in Figs. 4 and 5, where we have considered a fully atomic initial state in order to highlight the phenomena. We have also analyzed the quantum transport properties of the AN. The excitation is most likely to be found at the initial node, as expected. By evaluating the long-time average photonic occupation probability for different AN generations, we have discussed the interplay between the nodes and subnetworks thus showing their role on the system dynamics. At a given generation $n$, the nodes with $\gamma = 3$ are mostly connected with its correspondent hub node from the previous generation and with some other nodes having the same degree within local subnetworks. Furthermore, these properties hold recurrently as we increase the network size (see Fig. 8).

The JCH regime, $\kappa \approx \beta$, is characterized by a polariton interference which leads the system to roam between photonic and atomic degrees of freedom in a nontrivial way. The dynamics is neither strictly ruled by JC-like pairs of polaritons nor does the photonic mode propagate freely. Instead, for a

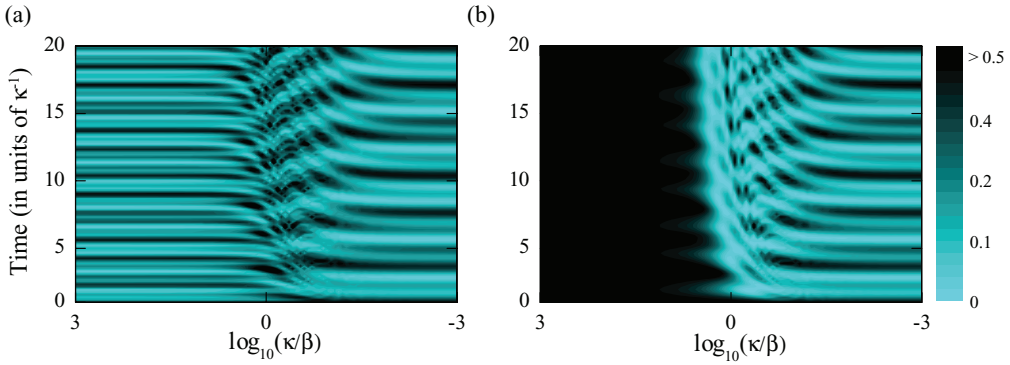


FIG. 10. (Color online) Comparison between atomic and photonic propagation dynamics from the large hopping regime, $\kappa/\beta = 10^3$, to the strong atom-field coupling regime, $\kappa/\beta = 10^{-3}$, for an initial single cavity state $|\psi_k(0)\rangle = |k\rangle \otimes (|g,1\rangle + |e,0\rangle)/\sqrt{2}$ prepared at $k = 4$. In (a), the photonic return probability, $\pi_{44}^{ph}$, and in (b), the atomic counterpart. System parameters are $n = 4$, $\omega_a = 0$, and $\omega_f = 0$. The middle range of $\kappa/\beta$ values is where the JCH regime overcomes.

given detuning, even if JC-like pairs of polaritons are set, other polaritons associated with different frequency levels on the JCH spectrum now contribute to the dynamics. It generates a splitting between photonic and atomic average occupation (Fig. 9) within each cavity. Such deviation can be avoided (at least in a particular cavity) by setting an appropriate atomic frequency in order to create a pair of JC-like polaritons strongly localized at the initial node.

The strong atom-field coupling regime, $\kappa \ll \beta$, is reached by the time such polariton interference is so robust that every field normal mode becomes coupled to its atomic analog and hence the photonic and atomic excitation propagate coherently through the network.

## V. CONCLUSIONS

Even at the single excitation subspace, the JCH model provides a rich dynamics. Moreover, the AN induces a peculiar spectrum and set of strongly localized eigenstates due solely to its topology, as we have considered uniform coupling parameters over the network. The structure self-similarity naturally reflects on the JCH model dynamics. As a result, the atomic excitation might not be stationary at the strong hopping regime even for large-size networks. Another appealing feature is the possibility of driving a specific set of polaritons to rule the dynamics, by a judicious tuning of the atomic transition frequency.

We have also discussed the continuous time quantum walk on the AN for different system sizes. For any initial state (fully localized at a specific node), the system will always carry a large amount of information about its initial conditions and will significantly propagate to a small set of nodes only. Further work along this direction should also consider other kinds of initial states, other than localized, where a much more complex dynamics arises.

Even though high-fidelity excitation transport protocols in a one-dimensional array of coupled cavities have been proposed [27,29], such regular structures induce mostly extended polaritons, which do not highlight all the features the single excitation JCH model can provide, in contrast to nonconventional complex structures, which, aside from the JCH model, might also shed light on the behavior of other many-body systems.

## ACKNOWLEDGMENTS

Fruitful discussions with F. Ciccarello are gratefully acknowledged. A.M.C.S. wishes to thank the National Institute of Science and Technology for Complex Systems. This work was supported by the CNPq (Brazilian agency).

[1] M. A. Nielsen and I. L. Chuang, *Quantum Computation and Quantum Information* (Cambridge University Press, Cambridge, England, 2000).
[2] J. Pachos and H. Walther, Phys. Rev. Lett. **89**, 187903 (2002).
[3] A. Blais, R.-S. Huang, A. Wallraff, S. M. Girvin, and R. J. Schoelkopf, Phys. Rev. A **69**, 062320 (2004).
[4] C.-H. Su, A. D. Greentree, W. J. Munro, K. Nemoto, and L. C. L. Hollenberg, Phys. Rev. A **78**, 062336 (2008).
[5] E. T. Jaynes and F. W. Cummings, Proc. IEEE **51**, 89 (1963).
[6] B. W. Shore and P. L. Knight, J. Mod. Optics **40**, 1195 (1993).
[7] D. K. Armani, T. J. Kippenberg, S. M. Spillane, and K. J. Vahala, Nature (London) **421**, 925 (2003).
[8] K. Hennessy, A. Badolato, M. Winger, D. Gerace, M. Atatue, S. Gulde, S. Falt, E. L. Hu, and A. Imamoglu, Nature (London) **445**, 896 (2007).
[9] A. Wallraff, D. I. Schuster, A. Blais, L. Frunzio, R. S. Huang, J. Majer, S. Kumar, S. M. Girvin, and R. J. Schoelkopf, Nature (London) **431**, 162 (2004).
[10] M. J. Hartmann, F. G. S. L. Brandão, and M. B. Plenio, Laser Photon. Rev. **2**, 527 (2008).
[11] A. Tomadin and R. Fazio, J. Opt. Soc. Am. B **27**, A130 (2010).
[12] A. D. Greentree, C. Tahan, J. H. Cole, and L. C. L. Hollenberg, Nat. Phys. **2**, 856 (2006).

[13] M. J. Hartmann, F. G. S. L. Brandão, and M. B. Plenio, Nat. Phys. **2**, 849 (2006).
[14] D. G. Angelakis, M. F. Santos, and S. Bose, Phys. Rev. A **76**, 031805(R) (2007).
[15] D. Rossini and R. Fazio, Phys. Rev. Lett. **99**, 186401 (2007).
[16] M. Aichhorn, M. Hohenadler, C. Tahan, and P. B. Littlewood, Phys. Rev. Lett. **100**, 216401 (2008).
[17] J. Koch and K. Le Hur, Phys. Rev. A **80**, 023811 (2009).
[18] P. Pippan, H. G. Evertz, and M. Hohenadler, Phys. Rev. A **80**, 033612 (2009).
[19] S. Schmidt and G. Blatter, Phys. Rev. Lett. **103**, 086403 (2009).
[20] M. Knap, E. Arrigoni, and W. von der Linden, Phys. Rev. B **81**, 104303 (2010).
[21] M. Hohenadler, M. Aichhorn, S. Schmidt, and L. Pollet, Phys. Rev. A **84**, 041608 (2011).
[22] J. I. Cirac, A. K. Ekert, S. F. Huelga, and C. Macchiavello, Phys. Rev. A **59**, 4249 (1999).
[23] D. G. Angelakis and S. Bose, J. Opt. Soc. Am. B **24**, 266 (2007).
[24] J. I. Cirac, P. Zoller, H. J. Kimble, and H. Mabuchi, Phys. Rev. Lett. **78**, 3221 (1997).
[25] S. Bose, D. G. Angelakis, and D. Burgarth, J. Mod. Opt. **54**, 2307 (2007).
[26] C. D. Ogden, E. K. Irish, and M. S. Kim, Phys. Rev. A **78**, 063805 (2008).
[27] M. I. Makin, J. H. Cole, C. D. Hill, A. D. Greentree, and L. C. L. Hollenberg, Phys. Rev. A **80**, 043842 (2009).
[28] F. Ciccarello, Phys. Rev. A **83**, 043802 (2011).
[29] Y.-L. Dong, S.-Q. Zhu, and W.-L. You, Phys. Rev. A **85**, 023833 (2012).
[30] D. J. Watts and S. H. Strogatz, Nature (London) **393**, 440 (1998).
[31] M. E. J. Newman, Phys. Rev. E **64**, 016132 (2001).
[32] V. Latora and M. Marchiori, Phys. Rev. Lett. **87**, 198701 (2001).
[33] B. J. Kim, H. Hong, and M. Y. Choi, Phys. Rev. B **68**, 014304 (2003).
[34] O. Mülken, V. Pernice, and A. Blumen, Phys. Rev. E **76**, 051125 (2007).
[35] J. S. Andrade, H. J. Herrmann, R. F. S. Andrade, and L. R. da Silva, Phys. Rev. Lett. **94**, 018702 (2005).
[36] I. N. de Oliveira, F. A. B. F. de Moura, M. L. Lyra, J. S. Andrade, and E. L. Albuquerque, Phys. Rev. E **79**, 016104 (2009).
[37] R. F. S. Andrade and H. J. Herrmann, Phys. Rev. E **71**, 056131 (2005).
[38] A. L. Cardoso, R. F. S. Andrade, and A. M. C. Souza, Phys. Rev. B **78**, 214202 (2008).
[39] A. M. C. Souza and H. Herrmann, Phys. Rev. B **75**, 054412 (2007).
[40] X.-P. Xu, W. Li, and F. Liu, Phys. Rev. E **78**, 052103 (2008).
[41] D. W. Boyd, Can. J. Math. **25**, 303 (1973).
[42] The AN has a self-similar structure where each subnetwork, generated by three new corner nodes, locally preserves the AN recurrence but breaks the degree group symmetry of the original AN (see Fig. 2).